Applied Energy 94 (2012) 166–173

Contents lists available at SciVerse ScienceDirect

Applied Energy

journal homepage: www.elsevier.com/locate/apenergy

Numerical study of a butanol/heptane fuelled Homogeneous Charge Compression Ignition (HCCI) engine utilizing negative valve overlap

Sona Visakhamoorthy [a], John Z. Wen [a,*], Siva Sivoththaman [b], Charles Robert Koch [c]

[a] Department of Mechanical and Mechatronics Engineering, University of Waterloo, 200 University Avenue West, Waterloo, ON, Canada N2L 3G1
[b] Department of Electrical and Computer Engineering, University of Waterloo, 200 University Avenue West, Waterloo, ON, Canada N2L 3G1
[c] Department of Mechanical Engineering, University of Alberta, Edmonton, AB, Canada T6G 2G8

ARTICLE INFO

Article history:
Received 10 November 2011
Received in revised form 16 January 2012
Accepted 17 January 2012
Available online 16 February 2012

Keywords:
HCCI
Butanol
Heptane
Multi-zone
Model
Negative valve overlap

ABSTRACT

The calibration and comparison to experimental data of a parallel computing multi-zone combustion model for simulating operational characteristics of an n-butanol/n-heptane fuelled Homogeneous Charge Compression Ignition (HCCI) engine utilizing the negative valve overlap (NVO) technology is described. The model is calibrated using one experimentally characterized operating point and by taking into account the major features of NVO. The model simulations at other four operating points closely match the cylinder pressure trace and heat release rates of the experiments. The unburned hydrocarbon emission is predicted to a reasonable level while NO_x (nitric oxide NO and nitrogen dioxide NO_2) formation is under-predicted. The difficulty in mapping the NO_x emission is attributed to the fact that the combustion model operates within the closed cycle period of engines and therefore does not capture the complexity of the charge stratification within the NVO equipped engine. Nevertheless, the trend of increasing NO_x levels with the increasing fraction of butanol in the fuel mixture is captured and the model is able to predict the pressure, heat release rates, and combustion phasing for the three fuel blends tested.

1. Introduction

Alternative energy technologies and renewable fuels are possible ways to reduce the transportation fuel usage. Homogeneous Charge Compression Ignition (HCCI) engines are a promising extension of the current internal combustion engine technology in that they offer a design where emission levels of Spark Ignition (SI) engines can be attained with the thermal efficiency of Compression Ignition (CI) engines [1]. In HCCI engines, which can be considered as hybrid engines between SI and CI engines, a premixed fuel–air charge is compressed until it autoignites. This technology can help reduce the environmental impacts of the increased transportation fuel usage by offering reduced NO_x (nitric oxide NO and nitrogen dioxide NO_2) and soot emissions while operating at near diesel-engine efficiencies. Another major benefit offered by these HCCI engines is the ability to combust a wide variety of fuels ranging from low calorific value fuels such as biomass derived gases to natural gas, alcohols, gasoline, and diesel [1–5]. Furthermore, many of these fuels can be combined as blends such as n-butanol/n-heptane, ethanol/n-heptane, and n-butanol/gasoline [6–11].

In HCCI engines a homogeneous air–fuel mixture is compression ignited with a relatively large amount of charge dilution. This results in low-temperature combustion, which subsequently produces low NO_x and less soot due to a lack of fuel-rich flame regions or localized high-temperature regions in the cylinder. Moreover, higher thermal efficiencies are possible due to the higher compression ratios required to autoignite these dilute air–fuel mixtures. However, one of the main challenges is that combustion phasing of HCCI engines is controlled by chemical kinetics and as such there is no specific ignition timing event as there is in SI or CI engines. Another challenge is the relatively high levels of Unburned Hydrocarbon (UHC) and CO (carbon monoxide) emissions [12–14]. These emissions primarily arise from the charge in the crevice regions and from a thin thermal boundary layer that forms along the in-cylinder surfaces. Other challenges include higher noise levels due to rapid Heat Release Rates (HRRs) at high loads and a relatively narrow engine operating range [1].

To improve ignition and combustion processes and to reduce the environmental impacts, various engine control strategies have been implemented on HCCI engines. These techniques include varying the level of the Exhaust Gas Recirculation (EGR), adjusting the equivalence ratio, changing the intake temperature, and implementing Variable Valve Actuation (VVA). Negative valve overlap (NVO) is a specific form of VVA where the exhaust valve is closed before all the exhaust has been completely evacuated from the cylinder, which traps variable amounts of hot combustion products

* Corresponding author. Tel.: +1 519 888 4567x38362; fax: +1 519 885 5862.
E-mail addresses: spvisakh@engmail.uwaterloo.ca (S. Visakhamoorthy), john.wen@uwaterloo.ca (J.Z. Wen), sivoththaman@uwaterloo.ca (S. Sivoththaman), bob.koch@ualberta.ca (C.R. Koch).

0306-2619/$ - see front matter © 2012 Elsevier Ltd. All rights reserved.
doi:10.1016/j.apenergy.2012.01.047

[15]. The actual NVO period is defined as the time during which both the inlet and exhaust valves are closed. This control strategy for HCCI engines allows for charge preheating by the trapped exhaust gases, which promotes autoignition and improves performance [16]. The complicated chemical and physical processes introduced by 'recycling' the trapped exhaust gases do bring about new challenges to theoretical and modeling studies.

To understand the details of the combustion process or to design model based control strategies for HCCI engines, appropriate simulation models must be developed. These simulation models can differ widely in terms of complexity and computational cost and can be broadly categorized into one of three groups: single zone models with chemical kinetics [17], multi-zone models with chemical kinetics [18,19], and Computational Fluid Dynamics (CFD) based models with chemical kinetics [20]. The simplest of these three groups of models is the single zone model with chemical kinetics where the entire charge mass is treated as a single lumped zone of homogeneous temperature, pressure, and species concentration. Reaction rates and species evolution are solved using chemical kinetics. These models tend to over-predict HRR and pressure rise rates while under-predicting certain emissions due to the assumptions inherent to such single zone models. For example, they lack any means of representing crevice regions and thermal boundary layers within the engine which are a significant source of CO and UHC emissions. To better differentiate among the bulk charge, thermal boundary layer, and crevice regions, multi-zone models are used. Here, the in-cylinder charge is broken down into concentric ring-like or individually lumped zones which are treated as stirred reactors. Each zone is homogeneous in terms of species concentrations and temperature and pressure distributions, but the zones are stratified from one another. This treatment allows for capturing the species and temperature gradients throughout the cylinder but requires more zones if a larger temperature gradient exists across the cylinder.

Since single and multiple zone models operate within the closed period of the engine cycle (between the Inlet Valve Closing (IVC) and the Exhaust Valve Opening (EVO)) the initial conditions of the combustion chamber (including the chemical compositions and temperature) at IVC are set by the user. Due to the difficulty in ascertaining the exact values of these initial conditions and the sensitive nature of HCCI combustion, this can lead to some inaccuracy in the model prediction. To reduce this error and improve the inputs to the model, single zone models may be augmented with full engine cycle simulations that calculate conditions up to IVC, at which the single zone model takes over until EVO [21]. Similarly, multi-zone models may be linked to a CFD solver such as KIVA which has been used to determine the initial gas mixture and temperature distribution prior to combustion. Typically at a certain piston position, the multi-zone model takes over based on the temperature profile that is calculated by the CFD code. Finally, there are pure CFD models where the chemical kinetics is fully implemented throughout the closed cycle period [20]. In these cases mass and heat transfer can be solved along with accurate turbulence modeling of the compressed gases. The CFD modeling provides insight into the specific engine features which promote turbulence such as in the squish area of the pistons. However, due to the level of details involved and depending on the mesh size, these simulations can be very computationally intensive. In addition, significant efforts are needed to produce complicated meshes for different engine geometries. Nevertheless, some research has been done to parallelize these models across computing clusters to reduce the computational time [20]. More fundamental work needs to be done, however, for implementing the CFD code in designing model based control strategies for HCCI engines.

As mentioned earlier, a major benefit of HCCI engines is their ability to combust a wide range of fuels. Fuels that have been experimentally tested and numerically simulated include Primary Reference Fuels (PRFs), natural gas, diesel, and methanol/ethanol/dimethyl-ether blends [1,22–24]. In this study, a HCCI engine fuelled with three n-butanol/n-heptane blends is used to validate a parallelized multi-zone model coupled with the detailed chemical kinetics. Since the fuel tested contains a fraction of large hydrocarbons (n-heptane), it exhibits low-temperature heat release [25]. This initial heat release occurs due to an increase in initial reaction rates caused by increasing temperature. Under such conditions, hydrogen is abstracted by oxygen from the fuel creating alkyl (R) and hydroperoxyl (HO_2) radicals. The alkyl radicals are consumed via two pathways which become dominant in the low-temperature heat release: alkylperoxy radical (RO_2) production and olefin production. At all temperatures, alkyl radical conversion to RO_2 is faster than olefin production. However, starting at approximately 700 K at 10 atm, the reverse RO_2·production reaction becomes dominant over the forward reaction thus increasing the production of alkyl radicals [26]. These alkyl radicals are then consumed via the olefin pathway. This overall increase in olefin production reduces the fuel consumption leading to the end of the low-temperature heat release region.

The objective of this work is to test and calibrate a recently developed multi-zone HCCI model [27] on a NVO equipped HCCI engine fuelled with varying ratios of bio-butanol/n-heptane and to compare the predictions with experimental data. The utility of the model for predicting the in-cylinder pressure, HRR, NO_x and unburned hydrocarbon emissions is examined.

2. Numerical simulation

The chemical mechanism chosen for this study is the one developed by Dagaut and Togbe [28]. This mechanism is based on the amalgamation and reduction of two discrete models: an n-butanol model [8] and two n-heptane models [29,30]. To predict the NO_x formation, the NO_x mechanism from GRI-Mech 2.11 is added to the above mechanism and this creates a reaction mechanism consisting of 200 species and 1805 reactions. The GRI-Mech 2.11 NO_x mechanism is selected as opposed to the that from GRI-Mech 3.0 since previous work [31,32] have indicated that GRI-Mech 3.0 over-predicts NO_x levels in partially premixed flames.

For this study, a 10-zone model with the detailed chemical kinetics is used to numerically solve the species, temperature and pressure evolution within the cylinder. It has been reported [27,33] that 10 zones are sufficient for solving the in-cylinder pressure trace, which is a major indicator of the engine performance. The selection of the number of zones is flexible but subject to the availability of the number of CPUs for parallel computing. This model operates within the closed cycle period of the engine and steps through species, temperature and pressure evolution at each incremental crank angle of one engine cycle. Heat transfer between zones and the cylinder walls is considered but the mass transfer between zones is not. There is, however, a mass loss due to blow-by and this is implemented by an equivalent loss of mass from all zones. Heat transfer coefficients are determined using the Woschni correlation which accounts for bulk gas velocity caused by the piston movement. Specifically, in order to describe the temperature gradient across the cylinder, a scaling factor is chosen with the selected volume of the hottest core zone. The original multi-zone numerical model is parallelized using the domain decomposition method and Fortran MPI (Message Passing Interface). This approach shares the computationally intensive step of solving the species evolution for each zone across multiple processors. It is found that running the parallelized model on a quad-core Intel i7 workstation results in runtimes reduced by approximately half in comparison to single-core computation of the serial model

Table 1
Description of adjustable model parameters.

Parameters
Intake temperature of the air fuel mixture
Cylinder wall temperature – assumed to remain spatially and temporally constant
Heat transfer scaling factor applied in the Woschni correlation
Blow-by losses
Fraction of the cylinder volume allocated to the core zone
Fraction of the trapped residual gases
Geometric ratio – how rapidly zones get thinner as they approach the wall
Thermal width – the temperature difference between the outermost and core zones

Table 2
Engine operating parameters.

Parameter (unit)	Value
Compression ratio (–)	12:1
Bore (mm)	97
Stroke (mm)	88.9
Connecting rod to crank arm ratio (–)	3.5996
Displacement volume (l)	0.653
IVO, IVC (deg, after the bottom dead center)	151°, 21°
EVO, EVC (deg, after the bottom dead center)	−100°, 130°
Engine speed (RPM)	1021
EGR (%)	0
Coolant temperature (C)	69–70
Intake temperature (C)	80
Equivalence ratio (–)	0.332, 0.345, 0.346, 0.357, 0.366
BVP (%)	12, 17, 22

on the same workstation. Typical serial mode runtimes are 80 min while parallelized runs take 40 min.

The model is calibrated against a given set of experimental data with a number of parameters adjusted. Exact experimental values for some of these parameters are generally unknown or difficult to determine from the existing experiment which is why they need to be calibrated. Once a suitable set of calibrated parameters has been determined for a single engine operating point, these parameters are left unchanged when the model is used as a predictive tool for other operating points. Table 1 shows a list of the adjustable parameters and their brief descriptions. Note: the geometric ratio, which is defined as the ratio of the thicknesses of the neighboring zones [34], is always set to 1 in this study.

3. Experimental data

The experimental apparatus is a single cylinder HCCI engine combusting n-butanol and n-heptane blends [25]. The engine test bed is a Ricardo Hydra Mark III using a Mercedes E550 cylinder head with variable valve timing. The fuel is injected into the intake runner. The intake air is preheated to a set temperature using a 600 W electrical band-type heater. The in-cylinder pressure is measured using a Kistler piezoelectric transducer and a K-type thermocouple with an accuracy of 2 °C is installed in the intake manifold and measures the intake temperature. Exhaust emissions are characterized using a 5-gas emissions test bench (Horriba CLA-510SS emission analyzer, which measures the gas concentrations using the chemiluminescent method). The exhaust emissions are sampled 5 cm downstream of the exhaust ports. NO_x emissions are measured with 1 ppm resolution, UHCs with 10 ppm resolution, and CO with 0.01% resolution. The crank angle position is recorded with 0.1° resolution using a BEI optical encoder.

Three Butanol Volume Percentages (BVPs) of the fuel at various equivalence ratios are tested with the intake temperature and engine speed held constant. They are BVP 12 (representing a volume fraction of 12% butanol in the fuel mixture), BVP17 and BVP 22. To calibrate and validate the simulation, five experimental operating points are selected, i.e., BVP 12 (φ = 0.332, 0.346), BVP 17 (φ = 0.345, 0.357) and BVP 22 (φ = 0.366). One operating point (BVP 17 at φ = 0.357) is used to calibrate the model while the other four are used for model validation. The experimental operating conditions of the engine are presented in Table 2. Some of these parameters (listed in Table 1) are adjusted during the model calibration, as shown later.

4. Results and discussion

4.1. Model calibration

As mentioned earlier, the parameters listed in Table 1 need to be calibrated using available experimental data since their values are not directly measured and cannot be easily determined. The operating point with BVP 17 at φ = 0.357 is used to calibrate the model. The calibration process matches pressure traces during the compression stroke by adjusting blow-by and matches ignition timing by varying the intake temperature. Then other parameters such as the temperature stratification, fraction of residual gases, and heat transfer scaling factor are modified to achieve a small error between the model prediction and experiment pressure trace over the entire CAD (Crank Angle Degree) range. During calibration, the intake temperature is not restricted to the measured intake manifold temperature since the significant amount of trapped gas, due to NVO, could cause preheating of the fresh air–fuel mixture charge. Blow-by is found to be negligible for this case and this is confirmed by literature [15]. It is important to note that this initial calibration of model parameters is conducted using the measured pressure trace only. The same set of model parameters is then used to investigate the trend of HRR and the formation of NO_x and UHC, which have required a further model calibration by adjusting the equivalence ratio, as discussed in Section 4.2.

The uncalibrated and calibrated pressure traces from the initial calibration are shown in Fig. 1 with the calibrated pressure trace matching experimental data quite well. The uncalibrated pressure trace does not take into account residual gases, blow-by losses, and the temperature stratification. The calibrated model parameters are specified in Table 3. It should be noted that the high residual gas fraction of 0.29 (29%) is caused by early closing of the exhaust valve to trap hot residuals. The cylinder wall temperature is not directly measured, but is estimated to be 20° above the coolant temperature. A relatively large core zone volume is selected with a greater heat transfer scaling factor. This implies that for this initial calibration case, there is a large volume of the hot fuel/air/gas mixture, mainly consisting of the residual gas, with a relatively uniform temperature in the cylinder. Between this core and the cylinder wall, there is a significant temperature gradient.

Using the calibrated pressure curve above, the HRR curve is calculated and shown in Fig. 2. Using the heat release analysis method outlined in [35], the net HRR is calculated by accounting for any heat transfer through the walls of the cylinder. The HRR curve generally shows adequate matching although the first-stage ignition is somewhat early and larger than experimental data. Experimentally, the first-stage ignition peaks at around 15CAD bTDC (before the Top Dead Center) whereas the simulation data indicates a peak at 20CAD bTDC. Discrepancies in predicting the correct ignition period may be due to the reaction mechanism or result from errors in setting initial conditions. It can be attributed to the model limitation in fully describing the NVO effects as well, as discussed later.

The measured NO_x level for the calibration case is 5.4 ppm [25] while the simulation result is 0.7 ppm. This under-prediction of the NO_x level can be explained by the thermal NO_x formation. In fact,

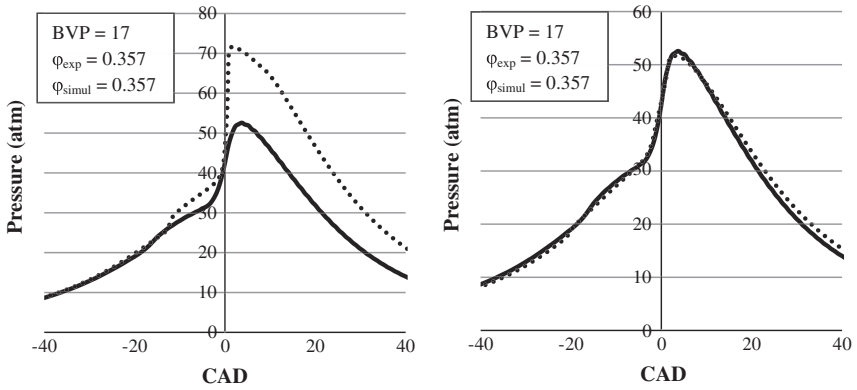

Fig. 1. Uncalibrated (left) and calibrated (right) predictions of the pressure trace for BVP 17. The dashed lines are the simulation results and the solid lines are the measured data.

Table 3
Calibrated model parameters.

Parameter (unit)	Value
Intake temperature (C)	122
Wall temperature (C)	90.0
Heat transfer scaling factor (–)	40.0
Blow by loss	Neglected
Core zone volume (–)	0.30
Residual gas fraction (–)	0.29
Thermal width (C)	0.0

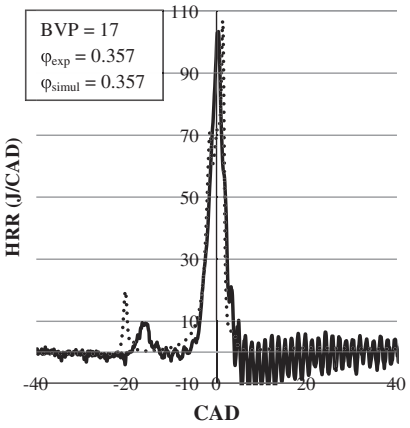

Fig. 2. The HRR curves for the calibration case BVP 17. The solid line is the measured data and the dashed line is the simulation result.

the predicted peak temperature in the cylinder ranges from 2100 K to 2250 K for individual cases and all these values are above the threshold temperature of the thermal NO_x formation. The NVO used in the experimental engine can introduce significant amounts of the inhomogeneity into the charge prior to ignition [36]. This inhomogeneity occurs in both the temperature distribution and species concentrations. Any fuel-rich regions caused by this inhomogeneity could cause localized hot spots and a higher production of NO_x. Those hot spots, especially when they occur across the cylinder and in individual zones, are not captured by the multi-zone model due to its underlying assumption of complete mixing between trapped gasses and the inducted fuel/air charge. The model also assumes the trapped residual gas with the same temperature of the intake charge (although the intake temperature is adjusted to account for the total energy balance). Since the in-cylinder temperature profile is difficult to measure, it is not available from the experiments. Otherwise, the locations of model zones could be set to better represent the temperature variation in cylinder. This could result in a better prediction of NO_x formation.

The predicted UHC emission of 226 ppm is much lower than the measured 1780 ppm in experiment. This difference is likely due to the thermal boundary layer in the numerical model being too thin. In other words, combustion is more complete in the numerical simulation and hence produces less UHC. This is observed during the model calibration as the expansion stroke of the simulation showed a slight deviation from the experiment. The deviation is likely caused by the excess energy remaining in the charge and can be reduced by increasing the size of the quenched thermal boundary layer. However, increasing the size of this layer in the simulation reduces the mass available for combustion and interferes with the proper combustion. Under experimental conditions, the implementation of NVO facilitates combustion with fuel injections occurring during the NVO period [16]. With NVO, trapped residuals can be oxidized during the NVO period and the fuel injected during this time facilitates combustion [16]. However, the simulation model only operates between IVC and EVO and cannot capture the NVO period and its associated phenomena. Thus, the combustion facilitation effect of NVO is not fully captured in the model and an increase in the size of the thermal boundary layer is also restricted.

4.2. Model limitations in predicting NVO

Previous work [27] involving similar combustion modeling has not been used to study experimental data from the NVO equipped HCCI engines. Due to the implementation of NVO, there could be variable amounts of trapped residual gases inside the cylinder depending on the valve timing. Using the experimental valve timing and engine specifications, the trapped gas percentage is determined using the ratio of the volume at the Exhaust Valve Closing (EVC) to the volume at IVC and is found to be 29%. This level of trapped gas is quite high but it is confirmed by other work using this same engine [25]. Such high levels of the trapped gas are possible because the exhaust valve is closed before the piston reaches TDC thus preventing all the exhaust gas from being evacuated. This trapped gas could have a fairly high temperature [36] and this should result in significant charge preheating. In addition, the trapped gas will modify the initial chemical compositions of the fuel/air mixture in the cylinder. The inclusion of such a large percentage of exhaust gases in the subsequent intake charge has different effects with regards to the model development. Firstly, since the multi-zone model does not account computationally for the temperature of trapped residual gases (it assumes the trapped gases

Table 4
Comparison of the model parameters before and after taking the NVO into account.

Original calibration		New calibration – accounts for NVO	
Parameter (unit)	Value	Parameter (unit)	Value
Intake temperature (°C)	122	Intake temperature (°C)	132
Heat transfer scaling factor (–)	40.0	Heat transfer scaling factor (–)	1.0
Core zone volume (–)	0.30	Core zone volume (–)	0.01
Thermal width (C)	0.0	Thermal width (C)	30.0

are at the same temperature of the intake charge), the intake charge temperature is specified as a manual input to the model. Secondly, the initial calibration assumes at IVC, there is a homogeneous mixture throughout the cylinder and there is no any temperature stratification in the computational domain. However, in practice, NVO could result in the significant inhomogeneity and stratification of the charge temperature and trapped residual gas at IVC [36]. This can lead to fuel-rich regions which will ignite sooner than the assumed homogeneous charge. Alternatively, increasing the overall equivalence ratio of the model could account for the earlier ignition caused by fuel-rich regions and applying the temperature stratification could better mimic the experimental situation. Finally, this model assumes that the residual gas is a complete combustion products constituting of CO_2, H_2O and N_2. However, the actual residual gas contains also NO_x and UHCs. These recycled NO_x and UHCs may contribute to combustion by effectively creating a slightly richer mixture in the subsequent cycle. This effect may be minimal for most operating points, but for points near the misfire limit, the recycling of unburned and partially burned reactants can significantly influence subsequent cycles [37]. The energy content of the intake charge should be increased when NVO is present due to the heat energy of the trapped residuals and any unburned or partially oxidized reactants.

With the increased energy content accounted, the model is recalibrated for the case (BVP 17, $\varphi = 0.357$) to improve matching of the predicted cylinder pressure with experimental data while relaxing constraints on the model parameters. The main difference between the experimental and original simulation pressure curves is a slight deviation during the expansion stroke likely due to more energy remaining in the charge during expansion in the simulation. This can be improved by forcing more mass into the outer zone to reduce the amount of mass which reacts. Doing so has two effects: it increases total unburned reactant emissions and reduces the peak pressure since there is less mass available for combustion. To further improve the model predictions, the equivalence ratio is increased by 14.8%. Not only does this aid in combustion, but it also represents the increase in equivalence ratio caused by trapped UHCs and any fuel-rich regions which may ignite early. Normally, for engines not implementing NVO, the equivalence ratio is not adjusted and is set to the experimental value [27]. Admittedly, a 14.8% increase is fairly large. Nevertheless, this increase, along with an increased mass in the outer zone, is the main adjustment between the new calibration and the original calibrated results.

Some other minor changes in model parameters are listed in Table 4. Note that the wall temperature and the residual gas fraction remain unchanged. The smaller heat transfer scaling factor is used together with a smaller core zone volume and a greater thermal width. The new calibration results in excellent pressure trace matching for the calibration case as shown in Fig. 3. Expansion stroke pressure trace matching is also improved compared to the original calibration. Using the pressure data, the HRR curve is calculated and matches the experimental results quite closely. In addition to exhibiting a good peak behavior, the HRR curve shows a significantly improved first-stage combustion timing and magnitude when compared to the experiment.

4.3. Model predictions

With this new set of calibrated parameters listed in Table 4, the other four operating points of the engine are simulated. No other parameters are changed during simulation except for BVP and the equivalence ratio. All equivalence ratios are raised by 14.8% above the experimental values.

For the four validation points the simulation results match closely to the experimental results except for a quite small deviation during the expansion strokes of the predicted pressure traces, as shown in Fig. 4. These simulation results capture the overall trends of the system with a good prediction of the cool flame activity. For example, changing from $\varphi = 0.332$ to $\varphi = 0.346$ with BVP12 shows an increase in the peak pressure which is expected due to the richer mixture, although the low-temperature HRR remains constant, as shown in Fig. 5. All HRR curves in Fig. 5 show excellent main-ignition timing and magnitudes and very good low temperature heat release timing and magnitudes. The effect of increasing equivalence ratios on the cool flame activity for a given BVP will be discussed later.

From the measured data, for a given BVP, HRR curves for various equivalence ratios exhibit nearly identical low-temperature HRR, but have varying high-temperature HRR. In other words, the equivalence ratio has little effect on the cool flame activity for a given BVP. This same trend is observed in the simulation predictions.

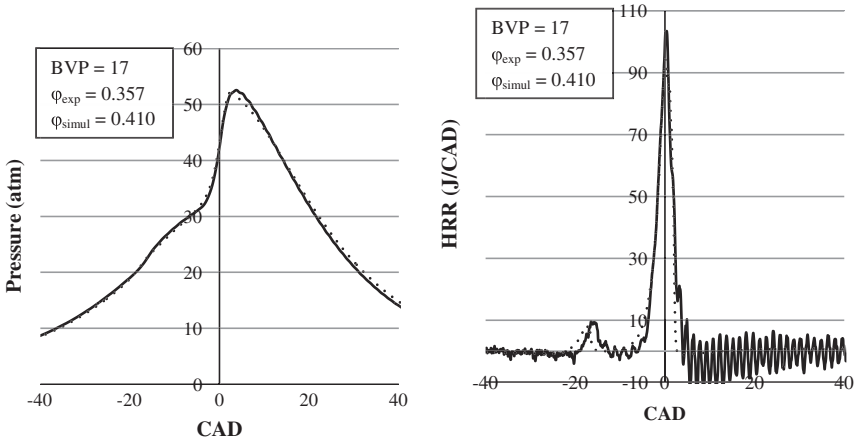

Fig. 3. Pressure and HRR curves for the improved calibration case. The solid lines are the measured data and the dashed lines are the simulation results.

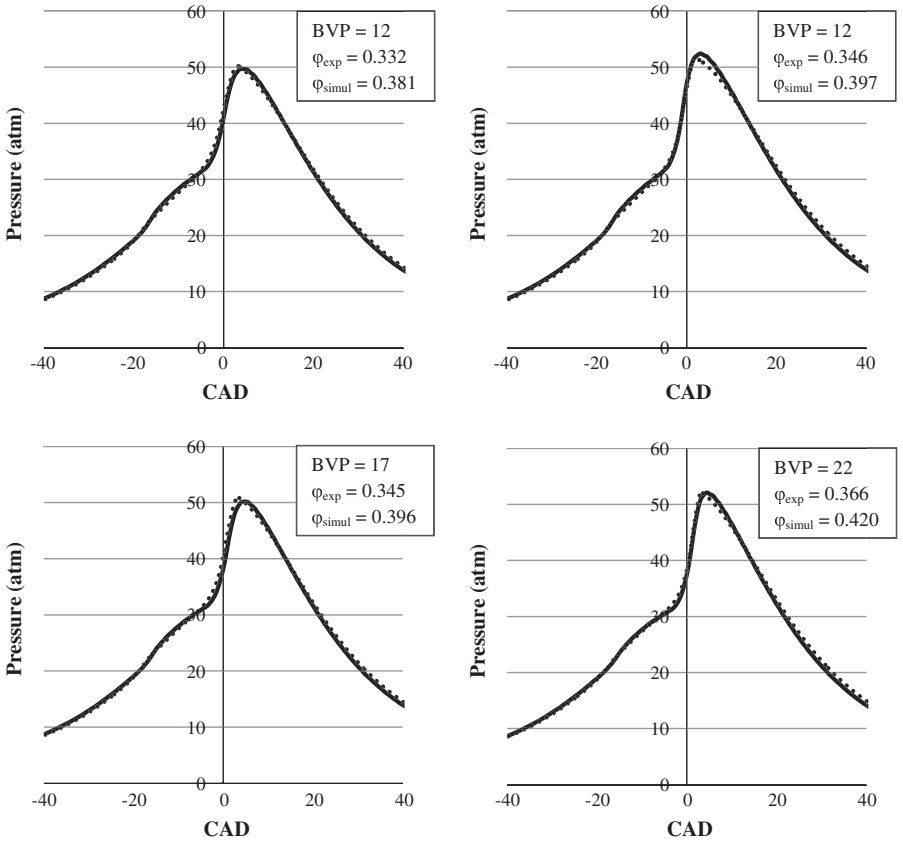

Fig. 4. Predicted pressure traces for the four validation points. The solid lines are the measured data and the dashed lines are the simulation results.

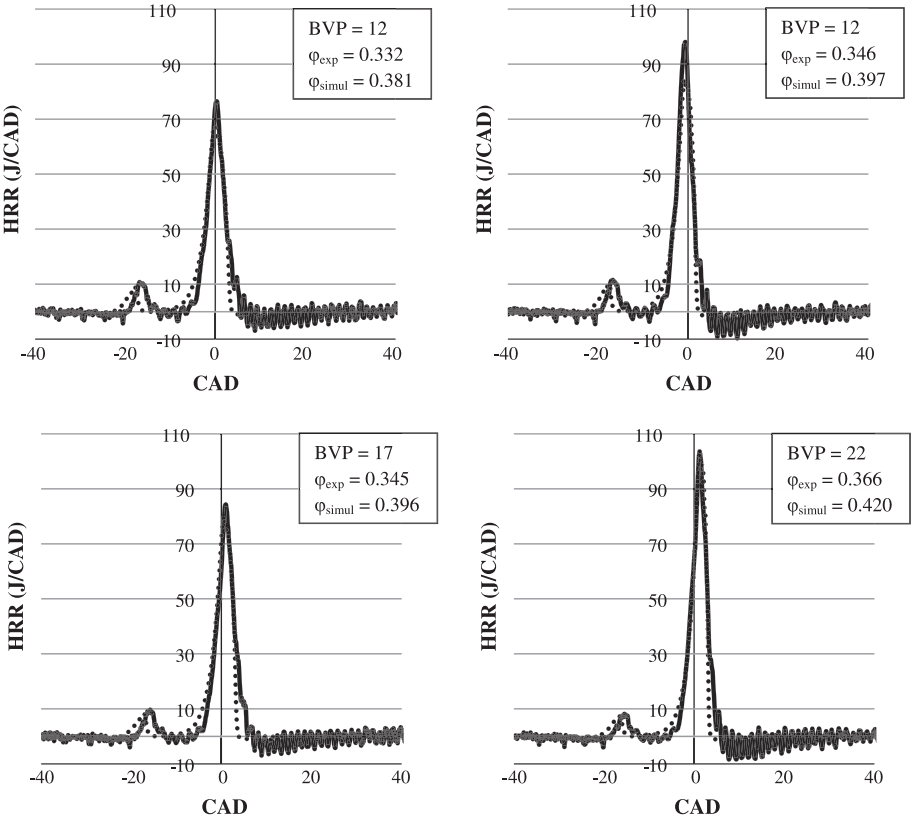

Fig. 5. HRR curves for the four operating points. The solid lines are the measured data and the dashed lines are the simulation results.

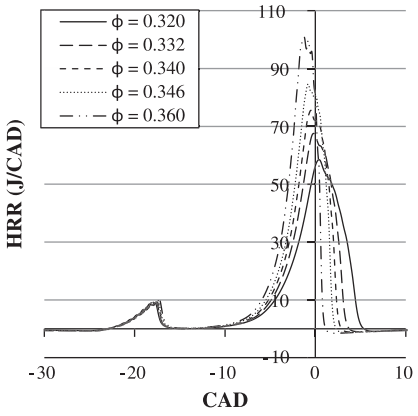

Fig. 6. The simulated HRR curves with varying equivalence ratios for BVP 12.

Table 5
Experimental and simulation emissions.

BVP	φ	NO_x		UHC	
		Simulation (ppm)	Experimental (ppm)	Simulation (ppm)	Experimental (ppm)
12	0.322	0.60	5.5	492	1851
12	0.346	0.54	5.4	503	1746
17	0.345	0.55	5.3	521	1877
17	0.357	0.53	5.4	531	1780
22	0.366	0.52	5.1	558	1845

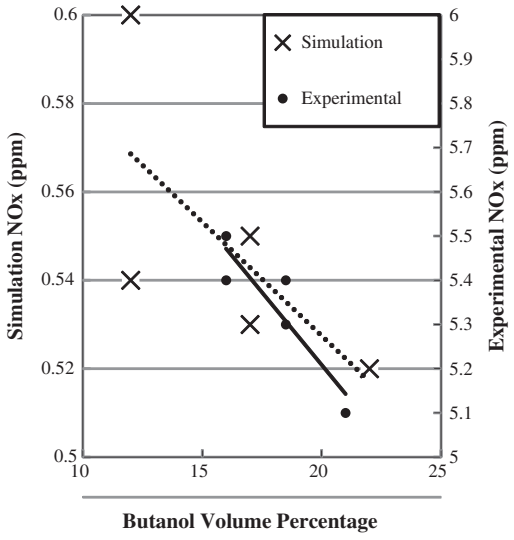

Fig. 7. NO_x trends in experimental data and simulation for a number of engine operating points listed in Table 5. The linear lines are plotted to show trends in both the simulation (dotted) and the experiment (solid).

In addition to the two cases of φ = 0.332 and 0.346 at BVP 12, three more cases of φ = 0.320, 0.340, and 0.360 are simulated. The HRR curves for these five cases are shown in Fig. 6, which shows that varying the equivalence ratios for a fixed BVP of 12 does not bring about significant changes in the low-temperature heat release.

The UHC predictions for the four predictive cases are on the order of 500 ppm. These levels are close to the experiment when compared to the first set of calibration results and this is attributed to the increased mass in the outer zone (i.e., the cooler thermal boundary layer). UHC levels are however still lower than the measured data of around 1800 ppm. NO_x emissions for the four validation cases are approximately one order of magnitude lower than the reported experimental values (about 5 ppm) as shown in Table 5. As previously mentioned the model cannot capture the inhomogeneity in species concentrations, which leads to part of the model discrepancy in predicting chemical species and temperature in the engine. Considering the three mechanisms of NO_x formation, namely fuel, prompt, and thermal, NO_x formation from fuel sources is unlikely in this study as there is no fuel bound nitrogen. The prompt NO_x is not found in the simulation results and this agrees with the previous finding that this mechanism was primarily observed in fuel-rich flames where hydrocarbon groups react with nitrogen to form Hydrogen Cyanide (HCN). The only effective mechanism, therefore, is thermal NO_x. It is interesting to see that as BVP is increased, NO_x levels decrease (Fig. 7) and this is likely due to a reduction in peak in-cylinder temperatures although no experimental temperature measurements are available to confirm this. This same trend is observed in the simulation results. The NO_x trend can be also affected by the discrepancy in predicting certain chemical species such as N_2 and O_2 under engine conditions with NVO. Again, the model has limitations in describing NVO equipped HCCI engines. Nevertheless, even though the simulation results underpredict NO_x levels, the model is useful for capturing overall trends as shown in Fig. 7.

5. Conclusions

A numerical multi-zone combustion model of an n-butanol/n-heptane fuelled HCCI engine utilizing NVO is studied. After calibrating the model to one operating point the simulations are run to predict the pressure traces and heat release rates for a number of operating points which are then compared to experimental data. The model is calibrated to account for major effects of NVO on the initial model conditions at IVC. The resulting calibrated model produces pressure traces and the HRR curves that closely match the experimental results at all five operating points. However simulated NO_x emissions are under-predicted compared to the experiment and this is attributed to the model limitation of not being able to capture the significant inhomogeneity of temperature and chemical compositions in the practical engine equipped with NVO. Similarly, the unburned hydrocarbon emissions are underpredicted but their predictions are improved when the major effects of NVO are accounted for during model calibration. Since the combustion model only operates for the closed valve period of the engine cycle, it cannot completely capture the combustion and emission effects of NVO. Nevertheless, calibration of the input parameters of the model to account for some aspects of NVO does result in excellent pressure trace and HRR predictions. This suggests that the model can be used as a predictive tool for investigating in-cylinder pressure, heat release, and combustion phasing in NVO equipped HCCI engines fuelled with the different n-butanol/n-heptane blends.

Acknowledgements

The authors of this paper would like to acknowledge the financial support provided through the Auto21 project D301-DHC and through NSERC.

References

[1] Yao M, Zheng Z, Liu H. Progress and recent trends in homogeneous charge compression ignition (HCCI) engines. Progress Energy Combust Sci 2009;35:398–437.
[2] Yamasaki Y, Kanno M, Taura Y, Kaneko S. Study on biomass gas HCCI engine. SAE Int 2009;32:66.
[3] Haggith D, Sobiesiak A, Miller L, Przybyla G. Experimental indicated performance of a HCCI engine fuelled by simulated biomass gas. SAE Int 2010;01:1081.

[4] Nathan SS, Mallikarjuna JM, Ramesh A. An experimental study of the biogas-diesel HCCI mode of engine operation. Energy Convers Manage 2010;51:1347–53.
[5] Maurya RK, Agarwal AK. Experimental study of combustion and emission characteristics of ethanol fuelled port injected homogeneous charge compression ignition (HCCI) combustion engine. Appl Energy 2011;88:1169–80.
[6] Saisirirat P, Foucher F, Chanchaona S, Mounaim-Rousselle C. Spectroscopic measurements of low-temperature heat release for Homogeneous Combustion Compression Ignition (HCCI) n-Heptane/Alcohol mixture combustion. Energy Fuels 2010;24:5404–9.
[7] Saisirirat P, Togbe C, Chanchaona S, Foucher F, Mounaim-Rousselle C, Dagaut P. Auto-ignition and combustion characteristics in HCCI and JSR using 1-butanol/n-heptane and ethanol/n-heptane blends. Proc Combust Inst 2011;33:3007–14.
[8] Dagaut P, Togbe C. Oxidation kinetics of butanol-gasoline surrogate mixtures in a jet-stirred reactor: experimental and modeling study. Fuel 2008;87:3313–21.
[9] Maurya RK, Agarwal AK. Statistical analysis of the cyclic variations of heat release parameters in HCCI combustion of methanol and gasoline. Appl Energy 2012;89:228–36.
[10] Fathi M, Saray RK, Checkel MD. The influence of Exhaust Gas Recirculation (EGR) on combustion and emissions of n-heptane/natural gas fueled homogeneous charge compression ignition (HCCI) engines. Appl Energy 2011;88:4719–24.
[11] Wu H-W, Wang R-H, Ou D-J, Chen Y-C, Chen T-y. Reduction of smoke and nitrogen oxides of a partial HCCI engine using premixed gasoline and ethanol with air. Appl Energy 2011;88:3882–90.
[12] Oakley A, Zhao H, Ladommatos N, Ma T. Experimental studies on controlled auto-ignition (CAI) combustion of gasoline in a 4-stroke engine. SAE Int 2001;01:1030.
[13] Christensen M, Johansson B, Einewall P. Homogeneous charge compression ignition (HCCI) using isooctane ethanol and natural gas – a comparison with spark ignition operation. SAE Int 1997:972874.
[14] Stanglmaier RH. TWR, Souder JS. HCCI operation of a dual-fuel natural gas engine for improved fuel efficiency and ultra-low NO_x emissions at low to moderate engine loads. SAE Int 2001;01:1897.
[15] Audet AD. Closed loop control of HCCI using camshaft phasing and dual fuels. Edmonton: University of Alberta; 2008.
[16] Aroonsrisopon T. Analysis of stratified charge operation and negative valve overlap operating using direct fuel injection in homogeneous charge compression ignition engines. Madison: University of Wisconsin-Madison; 2006.
[17] Flowers D, Aceves A, Smith R, Torres J, Girard J, Dibble R. HCCI in a CFR engine: experiments and detailed kinetic modeling. SAE Int 2000;01:0328.
[18] Aceves SM, Flowers DL, Westbrook CK, Smith JR, Pitz W. A multi-zone model for prediction of HCCI combustion and emissions. SAE Int 2000;01:0327.
[19] Visakhamoorthy S, Tzanetakis T, Haggith D, Sobiesiak A, Wen JZ. Numerical study of a homogeneous charge compression ignition (HCCI) engine fueled with biogas. Appl Energy 2012;92:437–46.
[20] Wang Z, Shuai S-J, Wang J-X. Multi-dimensional simulation of HCCI engine using parallel computation and chemical kinetics. SAE Int 2008;01:0966.
[21] Ogink R, Golovitchev V. Gasoling HCCI modeling: computer program combining detailed chemistry and gas exchange processes. SAE Int 2001;01:3614.
[22] Mack JH, Aceves SM, Dibble RW. Demonstrating direct use of wet ethanol in a homogeneous charge compression ignition (HCCI) engine. Energy 2009;34:782–7.
[23] Atkins MJ, Koch CR. The effect of fuel octane and dilutent on homogeneous charge compression ignition combustion. Proc Inst Mech Eng Part D – J Automob Eng 2005;219:665–75.
[24] Chen Z, Yao M, Zheng Z, Zhang Q. Experimental and numerical study of Methanol/Dimethyl Ether dual-fuel compound combustion. Energy Fuels 2009;23:2719–30.
[25] Shahbakhti M, Ghazimirsaied A, Audet A, Koch CR. Combustion characteristics of Butanol/n-Heptane blend fuels in an HCCI engine. in: Proceedings of combustion institute – Canadian section spring technical meeting. Ottawa; 2010.
[26] Zhao F, Asmus TW, Assanis DN, Dec JE, Eng JA, Najt PM. Homogeneous charge compression ignition (HCC) engines: key research and development issues. SAE Int 2003;03:646.
[27] Tzanetakis T, Singh P, Chen J-T, Thomson MJ, Koch CR. Knock limit prediction via multi-zone modelling of a primary reference fuel HCCI engine. Int J Veh Des 2010;54:47–72.
[28] Dagaut P, Togbe C. Experimental and modeling study of the kinetics of oxidation of Butanol-n-Heptane mixtures in a jet-stirred reactor. Energy Fuels 2009;23:3527–35.
[29] Curran HJ, Gaffuri P, Pitz WJ, Westbrook CK. A comprehensive modeling study of n-heptane oxidation. Combust Flame 1998;114:149–77.
[30] Seiser R, Pitsch H, Seshadri K, Pitz WJ, Curran HJ. Extinction and autoignition of n-heptane in counterflow configuration. Proc Combust Inst 2000;28:2029–37.
[31] Naha S, Aggarwal SK. Fuel effects on NO_x emissions in partially premixed flames. Combust Flame 2004;139:90–105.
[32] Barlow RS, Karpetis AN, Frank JH, Chen JY. Scalar profiles and NO formation in laminar opposed-flow partially premixed methane/air flames. Combust Flame 2001;127:2102–18.
[33] Flowers DL, Aceves SM, Martinez-Frias J, Dibble RW. Prediction of carbon monoxide and hydrocarbon emissions in iso-octane HCCI engine combustion using multizone simulations. Proc Combust Inst 2002;29:687–94.
[34] Tzanetakis T. Multi-zone modeling of a primary reference fuel HCCI Engine. Toronto: University of Toronto; 2006.
[35] Heywood JB. Internal combustion engine fundamentals. New York: McGraw-Hill; 1988.
[36] Rothamer DA, Snyder JA, Hanson RK, Steeper RR, Fitzgerald RP. Simultaneous imaging of exhaust gas residuals and temperature during HCCI combustion. Proc Combust Inst 2009;32:2869–76.
[37] Shahbakhti M, Koch CR. Characterizing the cyclic variability of ignition timing in a homogeneous charge compression ignition engine fuelled with n-heptane/iso-octane blend fuels. Int J Engine Res 2008;9:361–97.